Journal of Molecular Structure 1302 (2024) 137409

Contents lists available at ScienceDirect

Journal of Molecular Structure

journal homepage: www.elsevier.com/locate/molstr

Structural, magnetic and dielectric properties of green synthesized Ag doped $NiFe_2O_4$ spinel ferrite

Sunirmal Saha [a], Krutika L. Routray [a,*], Pritish Hota [a], Biswajita Dash [a], Satoru Yoshimura [b], Soumyaranjan Ratha [b], Traibhab Kumar Nayak [a]

[a] Department of Physics, C.V. Raman Global University, India
[b] Department of Materials Science, Graduate School of Engineering Science, Akita University, Japan

ARTICLE INFO

Keywords:
Ferrites
Green synthesis
Optical study
Impedance spectroscopy
AC conductivity

ABSTRACT

Ag-doped nano $NiFe_2O_4$ spinel ferrites were successfully synthesized using an environmentally friendly sol-gel technique. Comprehensive characterization of the obtained samples was carried out, employing techniques such as X-ray diffraction (XRD) and Fourier-transform infrared (FTIR) spectroscopy. The results from XRD and FTIR analyses unequivocally confirmed that the synthesized samples were of high purity and in a well-defined phase. Furthermore, examination of the samples through Field Emission Scanning Electron Microscopy (FESEM) revealed the formation of spherical grains, with an average grain size of 50 nm for pure $NiFe_2O_4$ nanoparticles and an increased size of 72 nm for the Ag-doped $NiFe_2O_4$ nanoparticles. Moreover, the investigation delved into the electrical conductivity and optical properties of these nanoferrites. It was noteworthy that the electrical conductivity demonstrated a significant enhancement in the case of Ag-doped $NiFe_2O_4$, further indicating the potential for improved performance. Magnetic analysis revealed a coercivity value (H_c) of 2.27 A/m for $NiFe_2O_4$, while the Ag-doped $NiFe_2O_4$ nanoparticles exhibited long-range ferromagnetic ordering. Additionally, optical absorption experiments disclosed an energy band gap of 1.75 eV for $NiFe_2O_4$, whereas the Ag-doped $NiFe_2O_4$ showcased a reduced energy band gap of 1.256 eV. These findings collectively contribute to a better understanding of the properties and potential applications of these materials in various technological domains.

1. Introduction

Spinel ferrite belong to the class of magnetic materials which is also referred to as cubic ferrites, have the general chemical formula MFe_2O_4 where M represents a divalent metal ion (Mn, Fe, Co, Ni, Cu, or Zn) [1–4]. Compared to hard magnetic hexaferrites which have also gained huge attention for microwave integration technology, permanent ferrite magnets, discovery of spinel ferrites have been the centre of attraction for material scientists [5–11]. Amongst the spinel ferrites, nickel ferrite $NiFe_2O_4$ (NFO) has gained wide attention owing to their significant porosity, remarkable resistivity and superior immersion polarization [12–15]. NFO are commonly used magnetic materials [16] and have considerable scope in the field of biomedical applications, such as tumor treatment, drug delivery [17,18], in the manufacturing of electronic materials [19,20]. In various industrial applications, NFO nanoparticles have been found to have extensive use as adsorbents and catalysts [21–23]. They also play a significant role in the manufacturing of electronic materials [24] and contribute to wastewater treatment efforts [25,26]. NFO have gained significance in contemporary sensor technology, including their application in biosensors, which find utility across diverse sectors, spanning from industrial applications to the realm of biomedicine [27]. Furthermore, NFO exhibit robust antimicrobial properties against specific pathogenic microorganisms [28]. Their notable attributes include high permeability, minimal dielectric loss, and consistent magnetization profiles in M-H curves [29,30]. The magnetic behavior of NFO relies on the compositions or the preference of the cation in either of the tetrahedral or octahedral sites. Material scientists have conveyed regarding incorporation of different rare earth and transition metals in NFO to improve its electrical and magnetic properties [31–34]. Almessiere et al. reported on doping La^{3+} and Y^{3+} to NFO composites and obtained high values of reflection loss and absorbing bandwidth which has potential applications for radar absorbing materials in the X-band. Along with they have reported on substitution of Dy^{3+}, Nb^{3+} in NFO and concluded to obtain enhanced

* Corresponding author.
E-mail address: krutika.routray@cvrp.edu.in (K.L. Routray).

https://doi.org/10.1016/j.molstruc.2023.137409
Received 1 August 2023; Received in revised form 20 December 2023; Accepted 22 December 2023
Available online 30 December 2023

magnetic and microwave characteristics of the nanomaterials to be used in microwave absorption [35–39]. Slimani et al. reported on room temperature superparamagnetic behavior and soft ferromagnetic characteristics below blocking temperature (T_B) for Eu^{3+} doped NFO composites making it useful for variety of devices operating at medium frequencies [40]. Considering this and also, silver (Ag) being the most commercialized nanomaterial, incorporation of Ag to NFO can enhance its electrical and magnetic characteristics as doping Ag in spinel ferrites enhances their magnetic and electrical properties, making them promising candidates for application such as high-density magnetic storage device and microwave devices [41–43]. Spinel ferrites with enhanced magnetic properties are used in the manufacturing of magnetic storage media, such as hard disk drives [44,45]. Spinel ferrites with improved electrical characteristics are valuable in microwave and high-frequency devices, such as circulators and isolators [46]. The introduction of Ag into nickel ferrite matrices has been explored in several studies, each aiming to elucidate its impact on the material's magnetic and electrical behaviors. Strong evidence for the existence of the Ag ions and the chemical interactions they make with the nickel and oxygen atoms in the ferrite structure can be seen from the structural characterizations [44, 45]. The unique electronic configuration and size of Ag ions make them particularly intriguing dopants for modifying the cation distribution and thereby the properties of nickel ferrite. This alteration can manifest in changes to the magnetic anisotropy, dielectric properties, and electrical conductivity, making Ag-doped nickel ferrites highly adaptable for emerging technologies. With the aid of this knowledge, it will be possible to create new materials with enhanced qualities and comprehend the characteristics of NFO doped with Ag. Reports indicate that doping of Ag creates a significant impact on the dielectric properties of ferrites [46–49,47]. As a result, Ag doped NFO is a potential material for devices like capacitors and filters that need a high dielectric constant. Syed Hamid Ud Din et al. reported on the most effective catalyst for the degradation of colored and colourless organic pollutants by doping Ag in NFO [50]. Adarshgowda et al. investigated on Ag doped NFO and showed superior antibacterial performance activity [48]. Ag doping can enhance other characteristics of NFO, including its magnetic and mechanical capabilities, in addition to enhance its dielectric constant and lowering its dielectric loss [50,48,51].

NFO can be synthesized through solid-state method, sol-gel auto combustion method [52,53], solvothermal method [54], hydrothermal method [55] *etc*. The sol–gel auto combustion method is preferred by researchers for synthesizing ferrite nanoparticles owing to its easy reproducibility, environmentally friendly method, and low-cost precursors than other metal oxides and safety. However, this method also comprises the use of oxidizing and reducing agents such as metal nitrates which acts as fuel [54]. So, in order to prevent the excessive usage of chemical fuel, green synthesis method has gained huge attention now-a-days [55]. The plant extract-based fuels are being used as a substitute to various reducing agents and have the ability to inhibit the chemical reaction as well as to complete it within few minutes.

Aloe vera (Aloe barbadensis miller) is known for its biocompatibility and low toxicity, making it a suitable choice for incorporating into materials that may have biological or biomedical applications [56]. This is particularly relevant in research in order to develop biocompatible materials by preventing the excessive usage of chemical fuel. Aloe vera being a natural and sustainable resource when used for material synthesis aligns with the principles of green chemistry and sustainability, which are increasingly important in materials science. Research suggests the incorporation of Aloe vera enhances certain characteristics of the material, such as electrical conductivity, dielectric properties, or magnetic behavior [55,56].

In the quest for enhancing the properties of Ag-doped nickel ferrite, the present investigation stands out with distinctive advantages when compared to existing literature works. This study delves into the comprehensive characterization of Ag-doped nickel ferrites, with a particular emphasis on understanding the cation distribution, magnetic parameters, dielectric behavior, and potential applications. What sets this research apart are the following key differentiators: Unlike many previous studies, this investigation undertakes a systematic analysis of the cation distribution within the Ag-doped nickel ferrite lattice, shedding light on the precise arrangement of Ag, Ni, Fe, and other cations in both A and B sites. The study offers a holistic approach to characterization, encompassing structural, magnetic, electrical, and dielectric properties. This thorough examination provides a comprehensive understanding of the material's behavior. The research extends beyond basic material properties and delves into the potential applications of Ag-doped nickel ferrites. This forward-thinking perspective aligns with the demands of modern technology. The investigation employs techniques including Rietveld refinement of XRD data, magnetic hysteresis measurements, dielectric characterization, and more, ensuring the reliability and accuracy of the results. Herein, we have adopted a novel and green method to synthesis pure as well as Ag incorporated NFO nanoparticles using Aloe vera plant extract assisted sol-gel method. In summary, the present study endeavors to unlock the full potential of Ag-doped nickel ferrites and offers a wealth of insights into their structural, magnetic, and electrical characteristics. The findings hold promise for a range of applications, making this research a significant contribution to the field of magnetic materials.

2. Experimental procedure

The Ag doped Nickel ferrites having chemical formula $Ni_xAg_{1-x}Fe_2O_4$ with $x = 0$, 0.05 were synthesized by the sol gel synthesis route using aloe vera extract. Nickel Nitrate [$Ni(NO_3)_2 \bullet 6H_2O$] (0.187 g), Ferric Nitrate [$Fe(NO_3)_3 \bullet 9H_2O$] (0.4837 g) and Silver Nitrate [$AgNO_3$] purchased from Sigma Aldrich (99.9 % purity) were used as precursors. Aloe vera (*Aloe barbadensis miller*) plant extract (2.5 ml) prepared was taken as reducing as well as oxidizing agent. The preparation of Aloe vera plant extract is described elsewhere [57]. By taking into account the principles of propellant chemistry, it is possible to determine the stoichiometric ratios of a redox mixture for a combustion process based on the ratios of the total oxidizing and reducing valences of the oxidizing agent and the valences of fuel. In this modified green sol-gel route, stoichiometric quantities of the nickel nitrate and iron nitrate were mixed with a M^{3+}/M^{2+} molar ratio of 2:1 and dissolved in 30 mL of the double distilled water. Aqueous solution of Nickel nitrate and Ferric nitrate was heated to 200 °C with continuous stirring. When the solution starts to seem homogenous, the Aloe vera plant gel (fuel) was added to it. Minutes later, a greyish, gel was formed which instantaneously got self-ignited to produce burnt ferrite powder. The formed powder was then continuously ground and sintered at 500 °C for 3 h. Correspondingly, Ag- NFO sample is synthesised using the same process as used to synthesis NFO, by taking the calculated amount of Ag dopant in the form of nitrate salt. The flowchart showing the synthesis procedure is illustrated in Fig. 1.

2.1. Characterization techniques

The structural characterisations were performed by room temperature X-ray diffraction (XRD) using Rigaku Ultima-IV X-ray Diffractometer and field emission scanning electron microscope (FESEM) (Nova NanoSEM-450), BIT Mesra. The elemental composition was determined by energy-dispersive X-ray spectroscopy (EDX) attached to FESEM. Dielectric measurements were carried out as a function of frequency (100 Hz to 1 MHz) and temperature (room temperature to 300 °C) using H20KI LCR meter (IM3570) for which1 mm thick and 13 mm diameter pellets were prepared using the manual hydraulic press. Thereafter high grade silver conducting paste (Sigma-Aldrich) was applied on both sides of pellets for better contact with the electrode. Optical properties of the prepared sample were observed by UV–Vis spectroscopy (UV–Vis spectrophotometer-UV-2600) and photoluminescence spectroscopy technique at room temperature within the

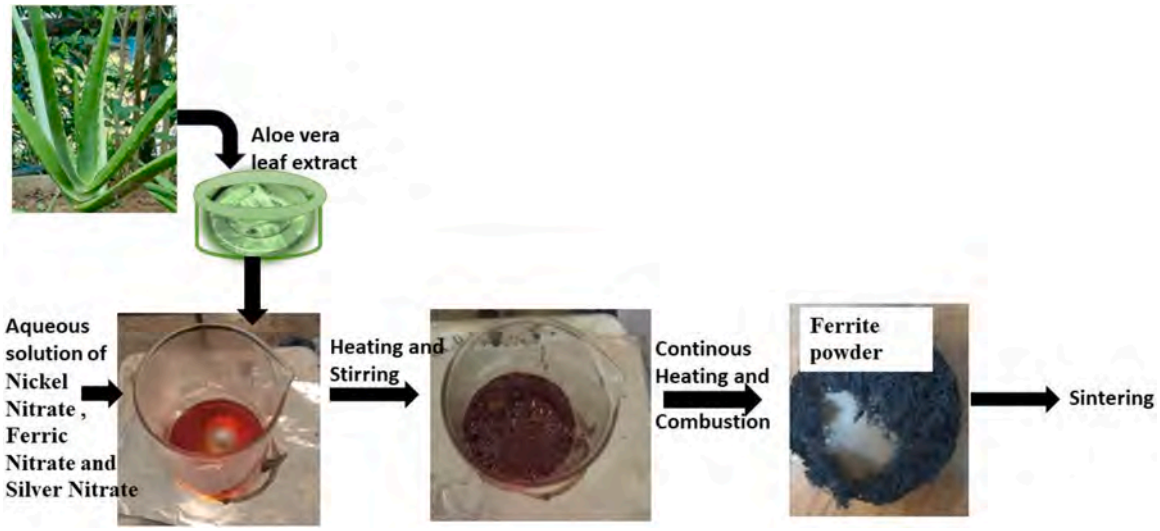

Fig. 1. Flowchart showing the green synthesis assisted solgel combustion method.

visible region range using 420 nm as the excitation wavelength on Edinburgh FS5 Spectro fluorometer. Photo-current measurements were carried out by using Keithley 6487 Pico ammeter/voltage source. To study the photocurrent response of the material in presence of visible light, the photocurrent–time measurements was carried out under visible-light illumination in an on-and-off cycle mode. Magnetic measurements were carried out at room temperature using vibrating sample magnetometer (VSM, Toei, VSM-5S).

3. Results and discussion

3.1. Structural analysis

It is clear that the as-burnt powder is slightly amorphous (Fig. 2a) but the sintered samples have a highly pure spinel structure. It is also indicated that the ferrite phase could be formed during combustion process. The broad peaks in XRD patterns indicate fine particle nature of the particles. The crystallite size of as-burnt powder was calculated from X-ray peak broadening of the (3 1 1) peak using Scherrer's formula [58]:

$$D = \frac{K\lambda}{\beta cos\theta} \quad (1)$$

where λ is the wavelength of the Cu Kα (1.5406 Å),

K is a dimensionless constant (Scherrer constant) and its value was assumed as 0.94 for the calculation of crystallite size

β = full width at half-maximum (FWHM) of the (3 1 1) peak in radians,

θ= Bragg's angle

The results showed that the crystallite sizes are in the range 50–60 nm for NFO and 70–80 nm for ANFO. The (hkl) values of the diffraction peaks are indexed as (220), (222), (311), (400), (331), (422), (511), (440) for NFO and Ag doped NFO (ANFO) are recorded with the help of X-Ray Powder Diffraction method and its Rietveld refinement for NFO (weighted profile factor R_{WP} = 9.51 %, and the goodness-of-fit χ^2 = 1.971) and ANFO weighted profile factor R_{WP} = 9.36 %, and the goodness-of-fit χ^2 = 2.316). From the XRD data in Fig. 2, it can be divulged that the reflection peaks are in close proximity and are sharp in nature. This approves the successful synthesis of single-phase nickel ferrite spinel with $Fd3^{-}m$ space group belonging to JCPDS PDF card no.10–0325 [47]. To acquire precise structural parameters, including cation occupancy at the available tetrahedral and octahedral sites within the spinel structure of our samples, as well as the lattice parameter, Rietveld refinement of the XRD patterns for each sample was conducted using the FullProf software. First and foremost global parameters such as 2θ–zero and background were refined and after Rietveld refinement of the XRD patterns were performed with the FULLPROF program in the

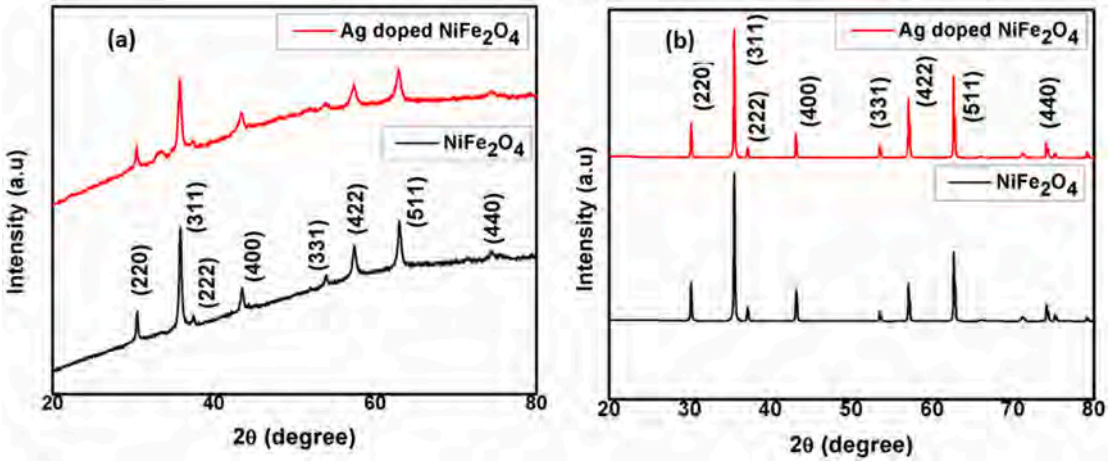

Fig. 2. X-ray diffraction pattern for the synthesized $NiFe_2O_4$ and Ag doped $NiFe_2O_4$ (a) before sintering (b) after sintering.

WINPLOTR suite of programs. The Rietveld-refined XRD patterns for the samples can be found in Fig. 3. The refined structural parameters, such as the lattice parameter and crystallite size, calculated and presented. The fitting parameters, including R_P, R_{WP}, R_{exp} (with values close to 20), and χ^2, exhibited highly satisfactory results, indicating an excellent fit to the experimental XRD patterns. The quality of fit of the experimental data was checked convoluting the reliability factors R_{WP}, R_{exp}, and goodness-of-fit χ^2 using the following distribution formulae:

$$R_{wp} = 100\left[\frac{\sum_{i=1} w_i \left|y_i - y_{c,i}\right|^2}{\sum_{i=1,n} w_i y_i^2}\right]^{1/2} \quad (2)$$

where y_i and $y_{c,i}$ are the observed and calculated profile intensities and w_i is a suitable weight.

$$R_{exp} = 100\left[\frac{N-P}{\sum_i w_i y_i^2}\right]^{1/2} \quad (3)$$

where $N - P$ is the number of degrees of freedom.

$$\chi^2 = \frac{R_{wp}}{R_{exp}} \quad (4)$$

Refinements were carried out till convergence is reached for the value of the goodness-of-ft close to 2. Through Rietveld refinement, the structural parameters were accurately determined by achieving the best fit with the XRD patterns. XRD intensities were computed following Burger's proposed formula [58],

$$I_{hkl} = |F_{hkl}|^2 P\, L_p \quad (5)$$

where I_{hkl} represents the integrated intensity, F_{hkl} stands for the structure factor, P signifies the multiplicity factor, and L_p represents the Lorentz polarization factor. The cation distributions for all compositions were determined by comparing the observed and calculated XRD intensity values across various cation combinations. The most sensitive Bragg planes, including (2 2 0), (3 1 1), (4 0 0), (331), and (4 2 2) were considered as they offer keen insight into cation distributions in both A and B sites. The resulting cation distribution for the $Ni_{1-x}Ag_xFe_2O_4$ system is presented in Table 1. Our findings reveal that Ag^{2+} cations occupy A-sites, while all Ni^{2+} cations are situated in B-sites. Additionally, the remaining A and B sites are occupied by Fe^{3+} cations. The maximum deviation in the obtained occupancy is estimated to be less than 3–4 %.

Lattice parameter has been calculated from following equation [59]

$$a = d * \left(h^2 + K^2 + l^2\right)^{1/2} \quad (6)$$

Table 1
Cation distribution of $NiFe_2O_4$ and Ag doped $NiFe_2O_4$.

Composition	A-site	B-site
0.0	$Ni^{2+}_{0.2}\ Fe^{3+}_{0.8}$	$Ni^{2+}_{0.8}\ Fe^{3+}_{1.2}$
0.05	$Ni^{2+}_{0.1}\ Ag^{2+}_{0.81}\ Fe^{3+}_{1.09}$	$Ni^{2+}_{0.09}\ Fe^{3+}_{0.91}$

The crystallite size has been calculate using Debye-Scherer's formula mentioned in Eq. (1). The lattice constant value obtained from the Scherer's method was found to be 8.1 Å for NFO which on addition of Ag was found to be 8.4 Å. The increase in lattice constant can be attributed to the larger ionic radius of Ag ions compared to that of Ni ions. Both Ag^{2+} (ionic radius of 1.28 Å) and Ni (ionic radius of 0.78 Å) ions are larger than the interstices of the A-site (0.58 Å) and B-site (0.73 Å) in the spinel cubic structure. Consequently, when Ag or Ni ions are introduced into these interstices, it results in the expansion of the lattice [47]. Notably, the lattice expansion is more pronounced when Ni ions are replaced by Ag ions, owing to the larger radius of Ag ions compared to Ni ions. Thus, the substitution of Ni with Ag ions leads to an increase in the lattice parameter.

Also, the average crystallite size (D) was found to increase on incorporation of Ag metal. For pure NFO, D value was found to be approximately 45 nm and for ANFO it was around 78 nm. When a material's crystallite size is reduced to a nanoscale, in the order of a few nanometers, it falls within the realm of quantum mechanics. In this regime, the behavior of electrons and electron energy levels is significantly different from that of bulk materials. When the crystallite size is reduced to a nanoscale, the quantum confinement effect comes into play. When the size of the crystallites becomes comparable to or smaller than the de Broglie wavelength of electrons, the available energy levels become quantized. This means that the energy levels for electrons are restricted to discrete values, resulting in an increase in the energy gap between the valence and conduction bands, which corresponds to an increase in the band gap. When the band gap increases, the material becomes more transparent to lower-energy photons. This is why a reduction in crystallite size leads to a decline in the optical band gap and an increase in transparency in the visible and near-infrared regions of the electromagnetic spectrum. Smaller crystallites effectively "open up" the band gap, reducing the energy required for electrons to transition from the valence band to the conduction band. Therefore, the observed decrease in the optical band gap in nanoscale materials, attributed to the diminution of crystallite size, fundamentally transforms the material's optical characteristics at the nanoscale level. This is explained further in the optical studies. However, no extra peaks for Ag were observed in Ag-NFO sample which indicates that the dopants did not get implanted to

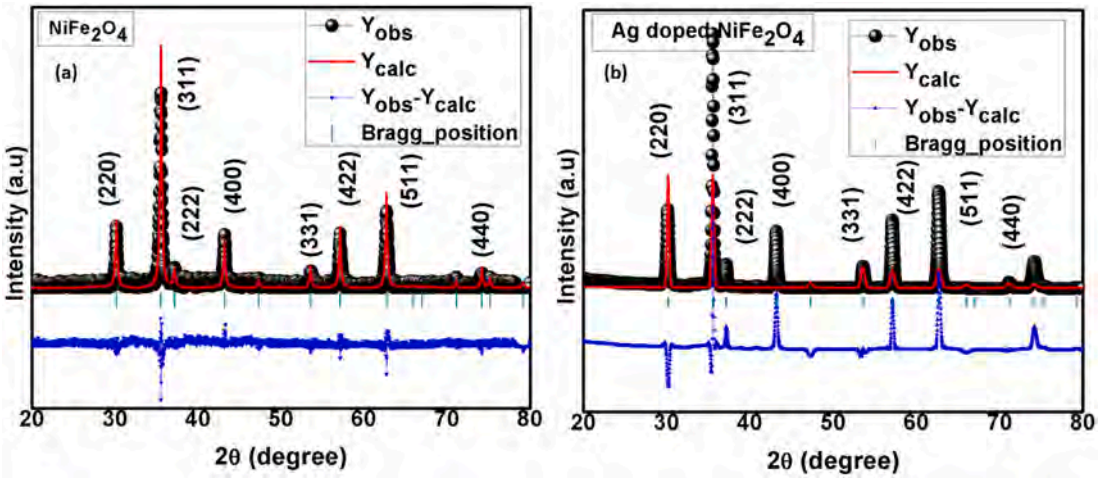

Fig. 3. Rietveld refinement X-ray diffraction pattern for the synthesized $NiFe_2O_4$ and Ag doped $NiFe_2O_4$.

the lattice but are clutched around the grain boundaries [59].

3.2. Morphological analysis

The morphological investigation included FESEM micro-imaging and EDX spectrum analysis, with findings presented in Figs. 4 and 5. For Ag-doped NFO, FESEM analysis in Fig. 4 portrays a distorted morphology of nanoparticles. The Ag content in the ferrite sample results in dramatic changes in morphology along with a variation in agglomeration The FESEM images clearly indicate an increase in the size of the nanoparticles within the aggregates, attributed to the presence of Ag. In Fig. 4(a), significant aggregates containing numerous particles are observed. The inset provides particle size distribution histograms, generated from a statistical analysis of over 100 particles. The distribution is fitted with a Gaussian curve, revealing a mean diameter of 43 $\pm$ 1.0 nm for NFO and 70 $\pm$ 1.0 nm for ANFO. A quantitative EDX shown in Fig. 5 is used to find the elemental composition of NFO and ANFO samples. The weight% of the elements is given as inset in the respective EDX spectrum. It confirms that the synthesized samples are nearly within the proper stoichiometric ratio and are consistent with the NFO and ANFO. Some peaks with same intensity were seen for all compositions in the same position, which indicated the presence of Ag. So, from the EDX spectra, samples are pure and there is no other impurity and that is in good agreement with the XRD.

3.3. Magnetic analysis

The magnetic properties of the NFO and ANFO were verified at room temperature using VSM magnetometer (Fig. 6). From the M-H curve, it is observed that NFO owing to its coercivity (H_c) value (2.27 A/m) is a soft magnetic material and the Ag doped NFO nanoparticles exhibit a long-range ferromagnetic ordering. The H_c obtained is minimal which is owed to the smaller grain size of the nanoparticles. These results agree with the results reported by Mahajan et.al. [60]. Satheeshkumar et.al. also observed higher value of H_c in Ag doped $CoFe_2O_4$ than pure $CoFe_2O_4$ (~1358 Oe) and they reported this due to influence of abundant aspects like magnetocrystalline anisotropy, microstrain, size distribution and magnetic domain size [61]. Nanoscale materials often exhibit size-dependent magnetic properties. Smaller grains have a higher surface area relative to their volume, which can introduce surface and interface effects that reduce H_c. In a magnetic material, the magnetic moments of individual grains or domains align to create a net magnetic moment. Smaller grains mean smaller domains, and they can be more easily realigned by an external magnetic field. Smaller grains have lower energy barriers for domain wall motion, making it easier for domains to change orientation, and thus, reducing H_c. In this case, the size of the nanoparticles is insufficient to overcome the thermal energy for which the energy barrier becomes less. Hence, the matinial has higher value of magnetism but lesser H_c. On incorporation of Ag, ferromagnetic behavior is observed, and the shape of the loop gets modified with doping Ag in nano-sized NFO. From the *M-H* loops, it can be divulged that magnetic moments and saturation magnetization (M_s) depends highly on the Ag content. The values of M_s obtained well agrees with the review report on various spinel ferrites including NFO where the M_s lies around 30 emu/gm. It is well known that the NFO is a magnetic material, but Ag is diamagnetic in nature, though, the diamagnetic behavior of Ag is insignificant in comparison to the magnetization of NFO. Consequently, NFO will be able to spin-polarize Ag in proximity close to the interface amid Au and NFO [62,63]. This results in intensification of net magnetic moment. Presence of Fe in NFO results in magnetic domains and the Fe spin alignment gets modified due to the delocalizing majority spin states [63]. This weakens the magnetic coupling of Fe spins. It is also seen that the coercivity (H_c) increased from 194 Oe for NFO to 268 Oe for Ag doped NFO. Typically, H_c provides information on the magneto-crystalline anisotropy of a material because it starts to form from the exchange anisotropy owing to the spin disorder occurring on the boundary of the particles. The introduction of Ag atoms into the material may lead to a dilution effect. As the concentration of Ag increases, the number of magnetic ions (Ni) relative to non-magnetic ions (Ag) decreases. This dilution effect can lead to a decrease in overall magnetization. Also, magnetic ions in the material interact with each other to create a magnetic moment. The introduction of Ag ions can disrupt these interactions, reducing the magnetic order and subsequently the magnetization. Literatures suggest that Ag induces antiferromagnetic behavior, hence it can counteract the alignment of magnetic moments and decrease magnetization [64]. Owing to high magnetization, high coercivity for strong data saving and small crystallite size for high density data storage, the synthesised material has potential for high density data storage devices.

3.4. Optical characterizations

Fig. 7a shows the optical absorption spectra of NFO and ANFO. The enhancement in ANFO is owed to the radiation absorbed by the Ag nanoparticles on exposure to light. A slight red shift was observed with incorporation of Ag. The band gap of the synthesised materials was investigated considering the absorption spectra using the Tauc-plot near edge optical absorption as shown in Fig. 7b [65]. From the Tauc plot, energy band gap (E_g) for NFO was calculated to be 2.67 eV and for ANFO was 2.53 eV. It is apparent from the Tauc plot that band gap decreases on incorporation of Ag although the decrease is very small. The decline in the optical band gap may be attributed to the reduction of crystallite

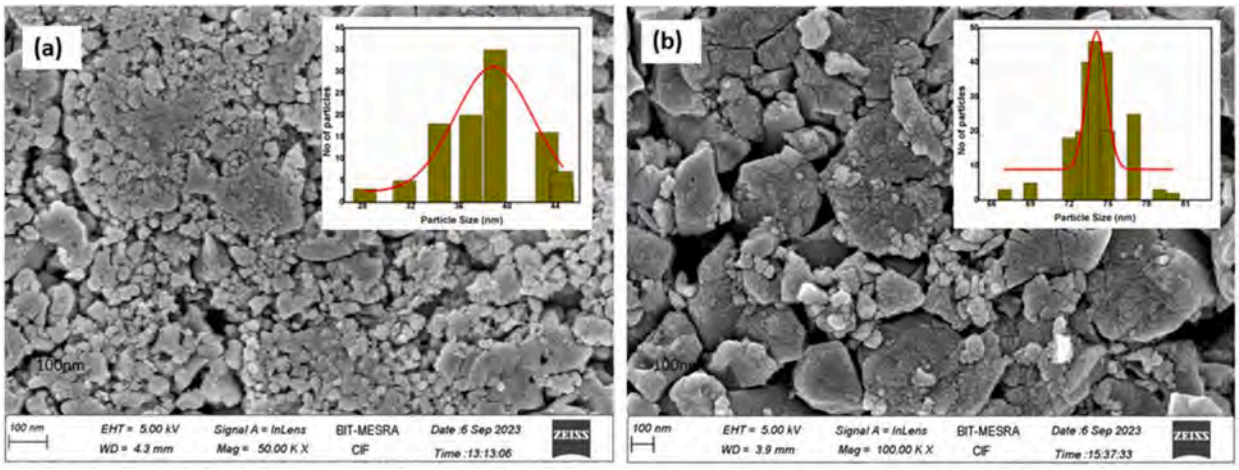

Fig 4. FESEM micrographs of the synthesized $NiFe_2O_4$ and Ag doped $NiFe_2O_4$ (inset showing the histograms).

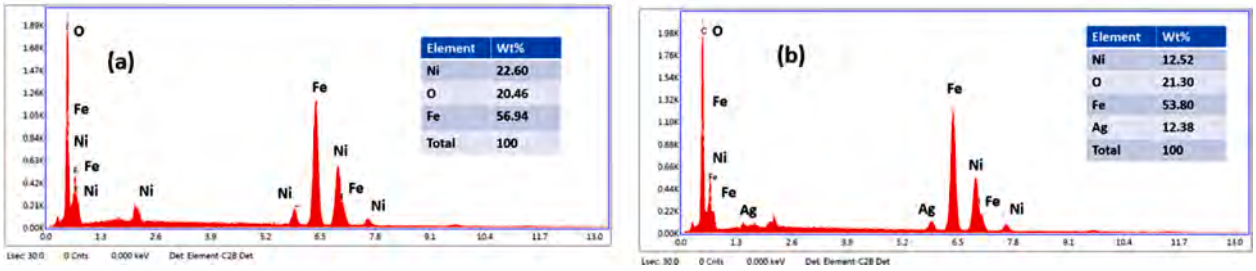

Fig 5. EDX spectra of the synthesized $NiFe_2O_4$ and Ag doped $NiFe_2O_4$.

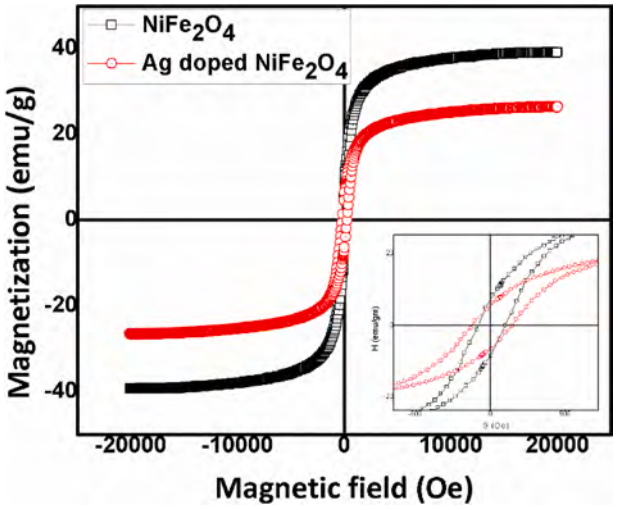

Fig. 6. Room temperature *M-H* curve for $NiFe_2O_4$ and Ag doped $NiFe_2O_4$.

size. This is also observed in the XRD data. This is indicative of the decrease in electron-hole recombination rate and concurrently improves the photovoltaic activity of the Ag doped NFO sample [66]. This reveals that Ag doped NFO samples display a significant visible-light response in photovoltaic applications.

3.5. Frequency dependence dielectric study

The room temperature variation of the dielectric constant (ε') and dielectric loss (ε'') for NFO and ANFO nano ferrites at in the frequency regime 100 Hz to 1 MHz is depicted in Fig. 8. A usual behaviour in the ε' is seen with frequency. With applied field and increase in value of frequency, the dielectric constant decreases exponentially and tends to approach a constant value at higher frequency. The dielectric constant is not a fixed value but is a function of the applied electric field and frequency. As the applied electric field or frequency increases, the dielectric constant of the material begins to approach a saturation point. At higher fields or frequencies, the polarization of the material reaches a limit, and further increases in the electric field have diminishing effects on the degree of polarization [67]. At sufficiently high frequencies, the dielectric constant tends to reach a constant value. This value is often referred to as the "high-frequency dielectric constant" or the "intrinsic dielectric constant." It represents the dielectric constant of the material when its polarization is saturated, and no further increase can be achieved with higher frequencies [68]. This frequency independent behaviour is observed in most of the ferrimagnetic material and is attributed to the conversion of Fe^{3+}ions to Fe^{2+} ions during the sintering process. It is seen that Fe^{3+}ions are more as compared to Fe^{2+} which renders dipolar ferrite material. Usually in ferrites, the exchange between both Fe^{3+} ions to Fe^{2+} ions occur aligning them with alternating field [68,69]. This causes a relaxation to the polarization. Also, the decrease in the dielectric constant is ascribed to the existence of space charge carriers which involve a fixed time interval to mark the axis in the way, the applied field acts. With increasing frequency, these space charge carriers lag to respond to the changing applied field resulting in decrease in dielectric constant.

The variation of ε'' as a function of frequency at room temperature is shown in Fig. 8b. As seen from the loss plot, the dielectric loss follows the same trend as dielectric constant. ε'' exhibits a rapid decline in the low-frequency region, followed by a gradual decrease in the high-frequency region, eventually reaching a state of nearly frequency independence. In the low-frequency domain, characterized by elevated resistivity attributable to grain boundaries, a heightened amount of energy is necessitated for electron exchange via interactions involving Fe^{3+}-O-Fe^{3+} within the octahedral sites. Conversely, the high-frequency region,

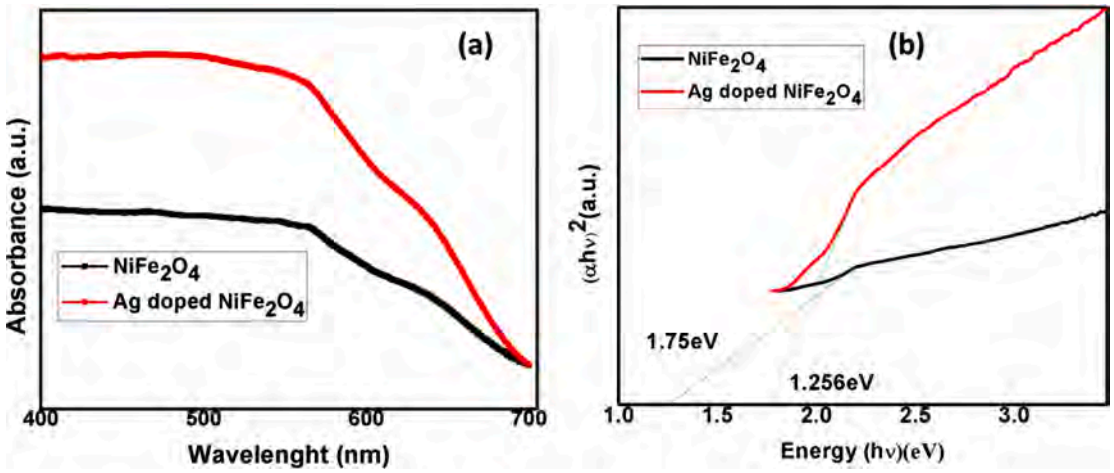

Fig. 7. (a) The optical absorption spectra (b) corresponding Tauc plot of $NiFe_2O_4$ and Ag doped $NiFe_2O_4$.

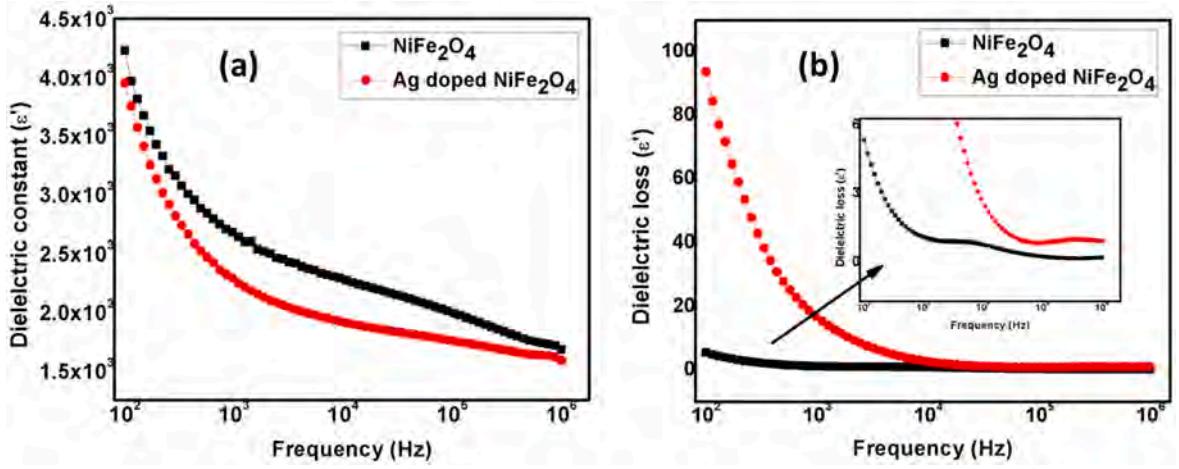

Fig. 8. (a) Dielectric constant (b) dielectric loss of $NiFe_2O_4$ and Ag doped $NiFe_2O_4$.

indicative of low resistivity within grains, demands a minimal energy input for electron transfer between two iron ions situated at the octahedral site [70]. Notably, ε'' illustrates a rapid initial decline in dielectric loss, with increasing frequency. The conduction mechanism in spinel ferrites is thought to involve electron hopping facilitated by the interaction of Fe^{3+}-O-Fe^{3+} with the octahedral site. Consequently, the observed maximum ε'' aligns with the scenario where the hopping frequency approximates the frequency of the applied electric field [71]. It is a fact that in ferrites, a strong correlation exists amongst the conduction behavior and the dielectric phenomenon. Hence, the decline in the of dielectric loss is ascribed to the hopping frequency of charge carriers which are incapable to track the alternative applied electric field at higher values of frequency. NFO is a semiconductor with a certain level of resistivity. The introduction of Ag, being a metal with high electrical conductivity, can significantly enhance the overall conductivity of the material. Higher conductivity typically results in increased dielectric losses due to enhanced energy dissipation. Also doping Ag nanoparticles influences the dynamics of charge carriers in NFO. The increased mobility of charge carriers, such as electrons, under the influence of an electric field can contribute to higher dielectric losses. It can be observed that ε'' shows a value of 5 for NFO whereas ε'' shows 99 value for Ag doped NFO as observed in Fig. 8b.

3.6. Impedance spectroscopy

A significant technique to analyse the electrical properties of ferrites is complex impedance spectroscopy (CIS). The room temperature variation of real part (Z') and imaginary part (Z'') of impedance of NFO and ANFO at varying frequency from 100 Hz to 1 MHz is presented in Fig. 9. From the impedance plot it is observed that the magnitude of Z' is higher at low value of frequency. This is attributed to the significant hopping of charge carriers between the localized ions. A diminution in Z' and Z'' is seen which is because of the conductivity at higher regime of frequency [72]. The decrease in Z'' in Fig. 9b with frequency signifies the existence of space charge polarization. The imaginary plot of Ag substituted NFO divulges an appearance of a peak indicating the existence of a relaxation mechanism. This peak is present in the lower frequency range and is ascribed to the space charge relaxation phenomenon of immobile charges or high annealing temperature [72].

Also, the electrical behaviour can be explained further by current-voltage (I-V) measurement. The current (I)- voltage (V) curves provide insight to the electrical conduction phenomenon and helps to determine the resistivity of the materials. I-V plot of ANFO is recorded at room temperature and shown in Fig. 10. From the plots it is seen that the behavior of the I-V pattern shifts from non-ohmic to ohmic in case of Ag doped NFO. This might be owed to the substitution of Ag which has resulted in agglomeration leading reduction in current and slight increase in the resistance value. Also, the transition might be due to the Ag particles being clutched to the grain boundaries.

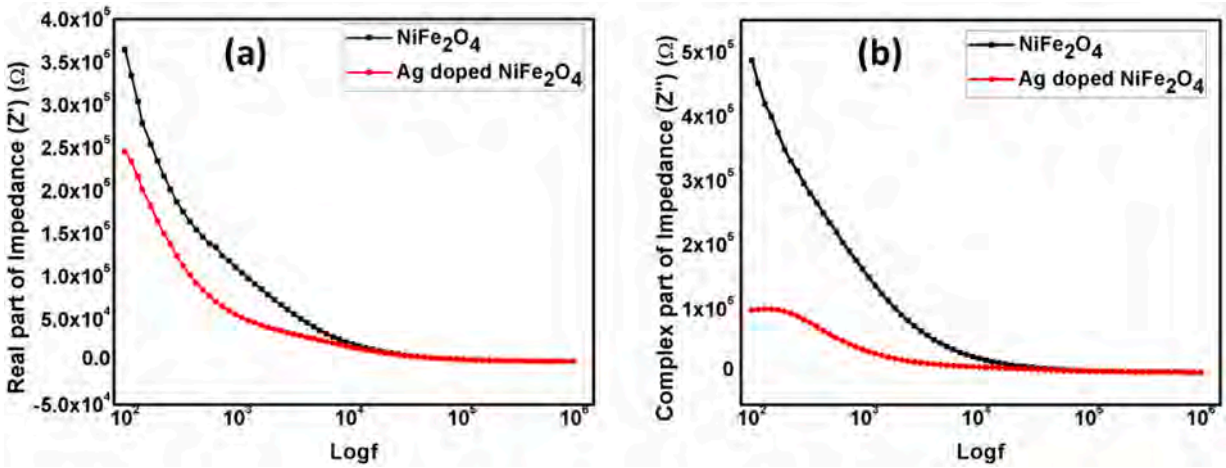

Fig. 9. Variation of (a) real part and (b) imaginary part of impedance spectra for $NiFe_2O_4$ and Ag doped $NiFe_2O_4$.

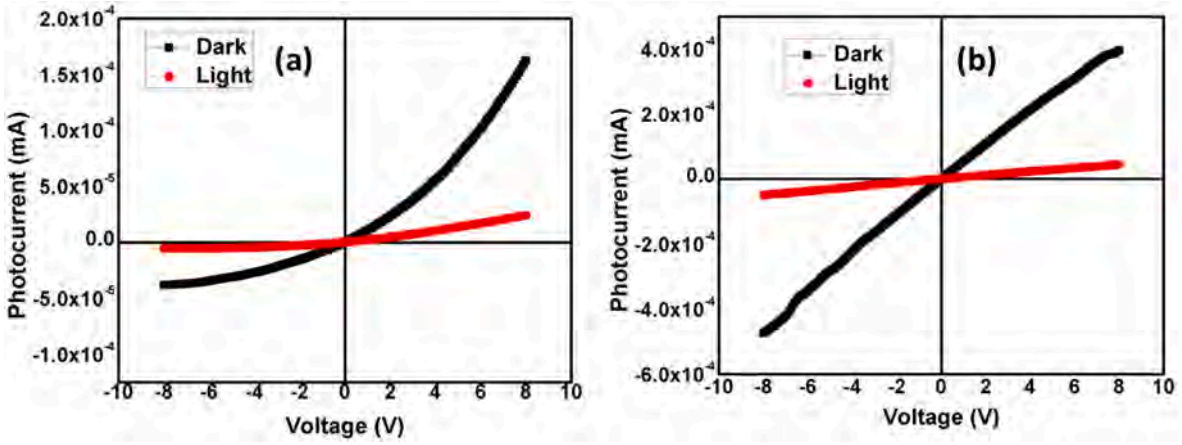

Fig. 10. I-V curve for (a) $NiFe_2O_4$ and (b) Ag doped $NiFe_2O_4$ as a function of frequency.

4. Conclusion

Nanoparticles of Ag substituted $NiFe_2O_4$ were successfully synthesized by sol-gel auto-combustion technique using Aloe vera extract as fuel. The XRD patterns divulge the establishment of single-phase cubic spinel ferrite, and the average crystallite size was found to increase from 50 nm for pure $NiFe_2O_4$ nanoparticles to 72 nm for Ag doped $NiFe_2O_4$ nanoparticles. FESEM micrographs revealed that after even after Ag substitution in NFO agglomeration was observed, the morphologies of all the samples obtained are with average particle sizes of 50 nm ranging to 70 nm in Ag doped NFO. The presence of the Ag^{2+} ions produced noticeable changes in the structural and morphological properties of NFO. The magnetic study displays a decrease in saturation magnetization with increasing coercivity with Ag doping. UV–VIS spectra show an enhancement in absorption peaks and that the band gap energy decreases with Ag substitution. The significantly high value of electrical resistivity with low dielectric loss values paves a way for the material to be used in transformer core and capacitor application. Frequency dependent dielectric properties show that on doping Ag, there occurs a decrease in the dielectric constant and is ascribed to the existence of space charge carriers which involve a fixed time interval to mark the axis in the way, the applied field acts. Impedance spectroscopy revealed that the magnitude of Z' is higher at low value of frequency owing to the significant hopping of charge carriers between the localized ions.

5. Motives and prospects for future research

Though, higher dielectric constant and low tan loss values obtained in the dielectric studies suggests the material to be used in high frequency devices. Also, owing to the high magnetization, high coercivity for strong data saving and small crystallite size for high density data storage, the synthesized material has potential for magnetic memory devices. However, magnetodielectric studies at high temperature and magnetic study at varying temperatures can yield a better perspective on its potential for high frequency devices. The upcoming styles in high frequency devices that are anticipated to influence the doped ferrites are mostly concerned on the synthesized methods, designing of the structures of the nanomaterials, and plan of magnetic and electric sensing arrangements. To come across the inevitability of high response and stability, it is suggested to enhance or alter the microstructure and adjust the stoichiometry of iron and doped material, put more emphasis on synthesizing porous structured materials and multi-component mixed ferrite. This study can be continued with new nanoparticles comprising of different Ag contents to divulge the optimal properties for dielectric and magnetic analysis. Moreover, involving a range of Ag concentrations can be used to establish a more comprehensive understanding of the studied properties and their relationship.

CRediT authorship contribution statement

Sunirmal Saha: Conceptualization, Data curation, Formal analysis, Funding acquisition, Investigation, Methodology, Project administration, Resources, Software, Supervision, Validation, Visualization, Writing – original draft, Writing – review & editing. **Krutika L. Routray:** Conceptualization, Data curation, Formal analysis, Funding acquisition, Investigation, Methodology, Project administration, Resources, Software, Supervision, Validation, Visualization, Writing – original draft, Writing – review & editing. **Pritish Hota:** Conceptualization, Data curation, Formal analysis, Funding acquisition, Investigation, Methodology, Project administration, Resources, Software, Supervision, Validation, Visualization, Writing – original draft, Writing – review & editing. **Biswajita Dash:** Conceptualization, Data curation, Formal analysis, Funding acquisition, Investigation, Methodology, Project administration, Resources, Software, Supervision, Validation, Visualization, Writing – original draft, Writing – review & editing. **Satoru Yoshimura:** Conceptualization, Data curation, Formal analysis, Funding acquisition, Investigation, Methodology, Project administration, Resources, Software, Supervision, Validation, Visualization, Writing – original draft, Writing – review & editing. **Soumyaranjan Ratha:** Conceptualization, Data curation, Formal analysis, Funding acquisition, Investigation, Methodology, Project administration, Resources, Software, Supervision, Validation, Visualization, Writing – original draft, Writing – review & editing. **Traibhab Kumar Nayak:** Conceptualization, Data curation, Formal analysis, Funding acquisition, Investigation, Methodology, Project administration, Resources, Software, Supervision, Validation, Visualization, Writing – original draft, Writing – review & editing.

Declaration of Competing Interest

The authors declare that they have no known competing financial interests or personal relationships that could have appeared to influence the work reported in this paper.

Data availability

Data will be made available on request.

References

[1] S.A. Prasad, M. Deepty, P.N. Ramesh, G. Prasad, K. Srinivasarao, C. Srinivas, K. V. Babu, E.R. Kumar, N.K. Mohan, D.L. Sastry, Synthesis of MFe2O4 (M= Mg2+, Zn2+, Mn2+) spinel ferrites and their structural, elastic and electron magnetic resonance properties, Ceram. Int. 44 (2018) 10517–10524, https://doi.org/10.1016/j.ceramint.2018.03.070.

[2] W. Cross, M. Kuznetsov, I. Parkin, Q. Pankhurst, Self-propagating high-temperature synthesis of ferrites MFe 2 O 4 (M= Mg, Ba, Co, Ni, Cu, Zn); reactions in an external magnetic field, J. Mater. Chem. 9 (1999) 2545–2552, https://doi.org/10.1039/A904431K.

[3] L. Affleck, M.D. Aguas, I.P. Parkin, Q.A. Pankhurst, M.V. Kuznetsov, Microstructural aspects of the self-propagating high-temperature synthesis of hexagonal barium ferrites in an external magnetic field, J. Mater. Chem. 10 (8) (2000) 1925–1932, https://doi.org/10.1039/B002431G.

[4] I.P. Parkin, M.V. Kuznetsov, Q.A. Pankhurst, J. Mater. Chem. 9 (1999) 273, https://doi.org/10.1039/A807123G. M. V. Kuznetsov, Q. A. Pankhurst, and I. P. Parkin, J. Phys. D, 1998, 31, 2886.

[5] M.A. Almessiere, Y. Slimani, H.S. El Sayed, A. Baykal, Morphology and magnetic traits of strontium nanohexaferrites: effects of manganese/yttrium co-substitution, J. Rare Earths 37 (7) (2019) 732–740. doi.org/10.1016/j.jre.2018.09.014.

[6] M.A. Almessiere, Y. Slimani, H.S. El Sayed, A. Baykal, I. Ercan, Microstructural and magnetic investigation of vanadium-substituted Sr-nanohexaferrite, J. Magn. Magn. Mater. 471 (2019) 124–132.

[7] Y. Slimani, B. Unal, M.A. Almessiere, E. Hannachi, G. Yasin, A. Baykal, I. Ercan, Role of WO3 nanoparticles in electrical and dielectric properties of BaTiO3–SrTiO3 ceramics, J. Mater. Sci. Mater. Electron. 31 (10) (2020) 7786–7797.

[8] M.H.A. Mhareb, Y. Slimani, Y.S. Alajerami, M.I. Sayyed, E. Lacomme, M. A Almessiere, Structural and radiation shielding properties of BaTiO3 ceramic with different concentrations of Bismuth and Ytterbium, Ceram. Int. 46 (18) (2020) 28877–28886.

[9] M.B. Salem, E. Hannachi, Y. Slimani, A. Hamrita, M. Zouaoui, L. Bessais, M. B. Salem, F.B. Azzouz, SiO2 nanoparticles addition effect on microstructure and pinning properties in YBa2Cu3Oy, Ceram. Int. 40 (3) (2014) 4953–4962.

[10] A. Hamrita, Y. Slimani, M.B. Salem, E. Hannachi, L. Bessais, F.B. Azzouz, M. B. Salem, 2014. Superconducting properties of polycrystalline YBa2Cu3O7–d prepared by sintering of ball-milled precursor powder, Ceram. Int. 40 (1) (2014) 1461–1470.

[11] A. Manikandan, M. Yogasundari, K. Thanrasu, A. Dinesh, K. Kanmani Raja, Y. Slimani, S.K. Jaganathan, R. Srinivasan, A. Baykal, Structural, morphological and optical properties of multifunctional magnetic-luminescent ZnO@ Fe3O4 nanocomposite, Phys. E: Low-Dimens. Syst. Nanostructures 124 (2020) 114291.

[12] Y. Wang, Q. Qi, G. Yin, W. Wang, D. Yu, Flexible, ultralight, and mechanically robust waterborne polyurethane/Ti3C2T x MXene/Nickel Ferrite Hybrid Aerogels For High-Performance Electromagnetic Interference Shielding, ACS Appl. Mater. Interfaces 13 (2021) 21831–21843, https://doi.org/10.1021/acsami.1c04962.

[13] N. Kumar, A. Kumar, G.M. Huang, W.W. Wu, T.Y. Tseng, Facile synthesis of mesoporous NiFe2O4/CNTs nanocomposite cathode material for high performance asymmetric pseudocapacitors, Appl. Surf. Sci. 433 (2018) 1100–1112, https://doi.org/10.1016/j.apsusc.2017.10.095.

[14] M.M. Sebastian, P. Velayudham, A. Schechter, N. Kalarikkal, Spinel nickel ferrite nanoparticles supported on a 1T/2H mixed-phase MoS2 heterostructured composite as a bifunctional electrocatalyst for oxygen evolution and oxygen reduction reactions, Energy Fuels 36 (2022) 7782–7794, https://doi.org/10.1021/acs.energyfuels.2c01191.

[15] S.B. Bandgar, M.M. Vadiyar, Y.C. Ling, J.Y. Chang, S.H. Han, A.V. Ghule, S. S. Kolekar, Metal precursor dependent synthesis of NiFe2O4 thin films for high-performance flexible symmetric supercapacitor, ACS Appl. Energy Mater. 1 (2018) 638–648, https://doi.org/10.1021/acsaem.7b00163.

[16] P. Sivakumar, R. Ramesh, A. Ramanand, S. Ponnusamy, C. Muthamizhchelvan, Synthesis and characterization of nickel ferrite magnetic nanoparticles, Mater. Res. Bull. 46 (12) (2011) 2208–2211.

[17] T. Ruthradevi, J. Akbar, G.S. Kumar, A. Thamizhavel, G.A. Kumar, R.K. Vatsa, G. C. Dannangoda, K.S. Martirosyan, E.K. Girija, Investigations on nickel ferrite embedded calcium phosphate nanoparticles for biomedical applications, J. Alloys Compd. 695 (2017) 3211–3219.

[18] X. Lasheras, M. Insausti, I. Gil de Muro, E. Garaio, F. Plazaola, M. Moros, L. De Matteis, J. M de la Fuente, L. Lezama, Chemical synthesis and magnetic properties of monodisperse nickel ferrite nanoparticles for biomedical applications, J. Phys. Chem. C 120 (6) (2016) 3492–3500.

[19] I.B.T. Silva, A.G. D'assuncao, J.B.L. Oliveira, J.R.F. Guerra, C.H.N Cordeiro, High-quality nickel ferrite synthesized by a modified sol–gel technique applied as microstrip patch antenna substrate, J. Electron. Mater. 49 (7) (2020) 4186–4194.

[20] E. Olsen, J. Thonstad, Nickel ferrite as inert anodes in aluminum electrolysis: part I Material fabrication and preliminary testing, J. Appl. Electrochem. 29 (1999) 293–299.

[21] W.A. Khoso, N. Haleem, M.A. Baig, Y Jamal, Synthesis, characterization, and heavy metal removal efficiency of nickel ferrite nanoparticles (NFN's), Sci. Rep. 11 (1) (2021) 3790.

[22] M. Naushad, T. Ahamad, B.M. Al-Maswari, A.A. Alqadami, S.M Alshehri, Nickel ferrite bearing nitrogen-doped mesoporous carbon as efficient adsorbent for the removal of highly toxic metal ions from aqueous medium, J. Chem. Eng. 330 (2017) 1351–1360.

[23] N.M. Mahmoodi, Nickel ferrite nanoparticle: synthesis, modification by surfactant, and dye removal ability, Water Air Soil Pollut. 224 (2013) 1–11.

[24] H. Zhao, Z. Zheng, K.W. Wong, S. Wang, B. Huang, D Li, Fabrication and electrochemical performance of nickel ferrite nanoparticles as anode material in lithium-ion batteries, Electrochem. Comm. 9 (10) (2007) 2606–2610.

[25] N. Fahoul, M.H. Sayadi, M.R. Rezaei, S. Homaeigohar, Nickel ferrite nanoparticles catalyzed dark fermentation of dairy wastewater for biohydrogen production, Bioresource Technol. Rep. 19 (2022) 101153.

[26] T.S. Saleh, A.K. Badawi, R.S. Salama, M.M.M. Mostafa, Design and development of novel composites containing nickel ferrites supported on activated carbon derived from agricultural wastes and its application in water remediation, Materials 16 (6) (2023) 2170.

[27] B. Baruwati, Studies on the Synthesis, Characterization, Surface Modification and Application of Nanocrystalline Nickel Ferrite, India Institute of Chemical Technology Hyderabad, 2007.

[28] J. Rawat, S. Rana, R. Srivastava, R.D.K. Misra, Antimicrobial activity of composite nanoparticles consisting of titania photocatalytic shell and nickel ferrite magnetic core, Mater. Sci. Eng.: C 27 (3) (2007) 540–545.

[29] S.K. Paswan, S. Kumari, M. Kar, A. Singh, H. Pathak, J.P. Borah, L. Kumar, Optimization of structure-property relationships in nickel ferrite nanoparticles annealed at different temperature, J. Phys. Chem. Solids 151 (2021) 109928.

[30] Z. Hou, J. Xiang, X. Zhang, L. Gong, J. Mi, X. Shen, K. Zhang, Microwave absorption properties of single-and double-layer absorbers based on electrospun nickel–zinc spinel ferrite and carbon nanofibers, J. Mater. Sci. Mater. Electron. 29 (2018) 12258–12268.

[31] B. Sarkar, B. Dalal, V. Dev Ashok, K. Chakrabarti, A. Mitra, S.K. De, Magnetic properties of mixed spinel BaTiO3-NiFe2O4 composites, J. Appl. Phys. 115 (2014) 123908, https://doi.org/10.1063/1.4869782.

[32] X. Zeng, Z. Hou, J. Ju, L. Gao, J. Zhang, Y. Peng, The cation distributions of Zn-doped normal spinel MgFe2O4 ferrite and its magnetic properties, Materials 15 (2022) 2422, https://doi.org/10.3390/ma15072422.

[33] V. Narayanaswamy, I.A. Al-Omari, A.S. Kamzin, B. Issa, H.O. Tekin, H. Khourshid, H. Kumar, A. Mallya, S. Sambasivam, I.M. Obaidat, Specific absorption rate dependency on the co2+ distribution and magnetic properties in coxmn1-XFe2O4 nanoparticles, Nanomaterials 11 (2021) 1231, https://doi.org/10.3390/nano11051231.

[34] Nlebedim, I.C., Melikhov, Y. and Jiles, D.C., 2014. Temperature dependence of magnetic Almessiere, Munirah Abdullah, Yassine Slimani, A. Demir Korkmaz, Abdulhadi Baykal, Hakan Güngüneş, Hüseyin Sözeri, Sagar E. Shirsath, S. Güner, S. Akhtar, and A. Manikandan. "Impact of La 3+ and Y 3+ Ion Substitutions on Structural, Magnetic and Microwave Properties of Ni 0.3 Cu 0.3Zn 0.4 Fe 2 O 4 Nanospinel Ferrites Synthesized Via Sonochemical Route." RSC advances 9, no. 53 (2019): 30671–30684.

[35] M.A. Almessiere, Y. Slimani, H. Güngüneş, S. Ali, A. Manikandan, I. Ercan, A. Baykal, A.V. Trukhanov, Magnetic attributes of NiFe2O4 nanoparticles: influence of dysprosium ions (Dy3+) substitution, Nanomaterials 9 (6) (2019) 820.

[36] Munirah Abdullah Almessiere, Yassine Slimani, Andrei V. Trukhanov, Abdulhadi Baykal, H. Gungunes, E.L. Trukhanova, V.G. Kostishin, Strong correlation between Dy3+ concentration, structure, magnetic and microwave properties of the [Ni0. 5Co0. 5](DyxFe2-x) O4 nanosized ferrites, J. Ind. Eng. Chem. 90 (2020) 251–259.

[37] M.A. Almessiere, Y. Slimani, S. Güner, A. Baykal, I. Ercan, Effect of dysprosium substitution on magnetic and structural properties of NiFe2O4 nanoparticles, J. Rare Earths 37 (8) (2019) 871–878.

[38] M.A. Almessiere, Y. Slimani, M. Sertkol, M. Nawaz, A. Sadaqat, A. Baykal, I. Ercan, B. Ozçelik, Effect of Nb3+ substitution on the structural, magnetic, and optical properties of Co0. 5Ni0. 5Fe2O4 nanoparticles, Nanomaterials 9 (3) (2019) 430.

[39] Y. Slimani, B. Unal, M.A. Almessiere, A.D. Korkmaz, S.E. Shirsath, G. Yasin, A. V. Trukhanov, A. Baykal, Investigation of structural and physical properties of Eu3 + ions substituted Ni0. 4Cu0. 2Zn0. 4Fe2O4 spinel ferrite nanoparticles prepared via sonochemical approach, Results Phys. 17 (2020) 103061.

[40] E. Grabowska, A. Zaleska, S. Sorgues, M. Kunst, A. Etcheberry, C. Colbeau-Justin, H. Remita, Modification of titanium (IV) dioxide with small silver nanoparticles: application in photocatalysis, J. Phys. Chem. C. 117 (2013) 1955–1962, https://doi.org/10.1021/jp3112183.

[41] N. Okasha, Influence of silver doping on the physical properties of Mg ferrites, J. Mater. Sci. 43 (2008) 4192–4197.

[42] B. Aslibeiki, Nanostructural, magnetic and electrical properties of Ag doped Mn-ferrite nanoparticles, Curr. Appl. Phys. 14 (12) (2014) 1659–1664.

[43] Y. Slimani, M.A. Almessiere, M. Nawaz, A. Baykal, S. Akhtar, I. Ercan, I. Belenli, Effect of bimetallic (Ca, Mg) substitution on magneto-optical properties of NiFe2O4 nanoparticles, Ceram. Int. 45 (5) (2019) 6021–6029.

[44] Y. Slimani, M.A. Almessiere, S. Güner, N.A. Tashkandi, A. Baykal, M.F. Sarac, M. Nawaz, I. Ercan, Calcination effect on the magneto-optical properties of vanadium substituted NiFe 2 O 4 nanoferrites, J. Mater. Sci. Mater. Electron. 30 (2019) 9143–9154.

[45] T. Ramesh, B. Sravanthi, K.K. Ganta, K. Praveena, J.N.V. Vardhan, A.R. Polu, Structural, magnetoelectric properties of multidoped Ni–Al ferrites for microwave circulator applications, Appl. Phys. A 128 (11) (2022) 957.

[46] A. Bhagat, A. Kokkiripati, B. Bhaduri, Synthesis of silver nanoparticles anchored on nickel ferrite/oxidized-graphite composite for the efficient reduction of aqueous P-nitrophenol, Inorg. Chem. Commun. 143 (2022) 109806, https://doi.org/10.1016/j.inoche.2022.109806.

[47] S.H. Din, M.H. Arshed, S. Ullah, P.O. Agboola, I. Shakir, A. Irshad, M. Shahid, Ag-doped nickel ferrites and their composite with rGO: synthesis, characterization, and solar light induced degradation of coloured and colourless effluents, Ceram. Int. 48 (2022) 15629–15639, https://doi.org/10.1016/j.ceramint.2022.02.097.

[48] B. Aslibeiki, Nanostructural, magnetic and electrical properties of Ag doped Mn-ferrite nanoparticles, Curr. Appl. Phys. 14 (2014) 1659–1664, https://doi.org/10.1016/j.cap.2014.09.025.

[49] A. Bhaskar, B.R. Kanth, S.R. Murthy, Electrical properties of Mn added MgCuZn ferrites prepared by microwave sintering method, J. Magn. Magn. 283 (2004) 109–116, https://doi.org/10.1016/j.jmmm.2004.05.039.

[50] N. Adarshgowda, H.B. Naik, R. Viswanath, G. Vishnu, A. Prathap, Bifunctional application of facile green-silver doped nickel ferrite nanoparticles via-combustion method, Chem. Data Collect. 47 (2023) 101066.

[51] Z. Zhang, G. Yao, X. Zhang, J. Ma, H. Lin, Synthesis and characterization of nickel ferrite nanoparticles via planetary ball milling assisted solid-state reaction, Ceram. Int. 41 (2015) 4523–4530, https://doi.org/10.1016/j.ceramint.2014.11.147.
[52] D.H. Chen, X.R. He, Synthesis of nickel ferrite nanoparticles by sol-gel method, Mater. Res. Bull. 36 (2001) 1369–1377, https://doi.org/10.1016/S0025-5408(01)00620-1.
[53] K. Maaz, S. Karim, A. Mumtaz, S.K. Hasanain, J. Liu, J.L. Duan, Synthesis and magnetic characterization of nickel ferrite nanoparticles prepared by co-precipitation route, J. Magn. Magn. 321 (2009) 1838–1842, https://doi.org/10.1016/j.jmmm.2008.11.098.
[54] K. Nejati, R. Zabihi, Preparation and magnetic properties of nano size nickel ferrite particles using hydrothermal method, Chem. Cent. J. 6 (2012) 1–6, https://doi.org/10.1186/1752-153X-6-23.
[55] A. Balaji, M.V. Vellayappan, A.A. John, A.P. Subramanian, S.K. Jaganathan, M. SelvaKumar, A.A. bin Mohd Faudzi, E. Supriyanto, M. Yusof, Biomaterials based nano-applications of Aloe vera and its perspective: a review, RSC Adv. 5 (105) (2015) 86199–86213.
[56] S.M. Rathod, S.V. Gaikwad, S.K. Gore, U.B. Tumberphale, S.F. Shaikh, M. Ubaidullah, B. Pandit, S.S. Jadhav, Ni–Ag ferrites synthesized by the sol-gel route using Aloe vera extract as a solvent: enhancement in structural, dielectric, magnetic, and optical properties, Physica B 661 (2023) (2023) 414944.
[57] S. Saha, K.L. Routray, D. Behera, Visible light driven photoluminescence activity of ZnFe2O4–Ag doped nanomaterials for photostability: green synthesis approach, Trans. Electr. Electron. Mater. (2023) 1–8.
[58] M.J. Buerger, J. Cryst. Struct. Anal.s (1960).
[59] T. Nawaz, M.B. Tahir, M. Sagir, K. Shahzad, A.M. Ali, H. Alrobei, Rapid photocatalytic degradation of dye and energy production through ternary BiVO4/Ag/NiFe2O4 nanocomposites under visible light irradiation, Ceram. Int. 48 (8) (2022) 11779–11785.
[60] P. Mahajan, A. Sharma, B. Kaur, N. Goyal, S. Gautam, Green synthesized (Ocimum sanctum and Allium sativum) Ag-doped cobalt ferrite nanoparticles for antibacterial application, Vacuum 161 (2019) 389–397.
[61] M.K. Satheeshkumar, E. Ranjith Kumar Ch Srinivas, N. Suriyanarayanan, M. Deepty, C.L. Prajapat, T.V. Chandrasekhar Rao, D.L Sastry, Study of structural, morphological and magnetic properties of Ag substituted cobalt ferrite nanoparticles prepared by honey assisted combustion method and evaluation of their antibacterial activity, J. Magn. Magn. Mater. 469 (2019) 691–697.
[62] S. Banerjee, S.O. Raja, M. Sardar, N. Gayathri, B. Ghosh, A. Dasgupta, Iron oxide nanoparticles coated with gold: enhanced magnetic moment due to interfacial effects, J. Appl. Phys. 109 (2011) 123902, https://doi.org/10.1063/1.3596760.
[63] A. Hao, M. Ismail, S. He, N. Qin, W. Huang, J. Wu, D. Bao, Improved unipolar resistive switching characteristics of Au-doped nickel ferrite magnetic thin films for nonvolatile memory applications, J. Alloys Compd. 732 (2018) 573–584, https://doi.org/10.1016/j.jallcom.2017.10.251.
[64] J.S. Kouvel, The ferromagnetic-antiferromagnetic properties of copper-manganese and silver-manganese alloys, J. Solid State Chem. 21 (1–2) (1961) 57–70.
[65] P.R. Jubu, F.K. Yam, V.M. Igba, K.P. Beh, Tauc-plot scale and extrapolation effect on bandgap estimation from UV–vis–NIR data–a case study of β-Ga2O3, J. Solid State Chem. 290 (2020) 121576, https://doi.org/10.1016/j.jssc.2020.121576.
[66] M.S. Sher Shah, A.R. Park, K. Zhang, J.H. Park, P.J. Yoo, Green synthesis of biphasic TiO2–reduced graphene oxide nanocomposites with highly enhanced photocatalytic activity, ACS Appl. Mater. Interfaces 4 (2012) 3893–3901, https://doi.org/10.1021/am301287m.
[67] R.N. Bhowmik, A.K. Sinha, Improvement of room temperature electric polarization and ferrimagnetic properties of Co1. 25Fe1. 75O4 ferrite by heat treatment, J. Magn. Magn. Mater. 421 (2017) 120–131.
[68] C.K. Ghosh, S. Malkhandi, M.K. Mitra, K.K. Chattopadhyay, Effect of Ni doping on the dielectric constant of ZnO and its frequency dependent exchange interaction, J. Phys. D Appl. Phys. 41 (24) (2008) 245113.
[69] D.R. Patil, B.K. Chougule, Effect of copper substitution on electrical and magnetic properties of NiFe2O4 ferrite, Mater. Chem. Phys. 117 (1) (2009) 35–40.
[70] Abdollah Hajalilou, Saiful Amri Mazlan, Kamyar Shameli, A comparative study of different concentrations of pure Zn powder effects on synthesis, structure, magnetic and microwave-absorbing properties in mechanically-alloyed Ni–Zn ferrite, J. Phys. Chem. Solids 96 (2016) 49–59.
[71] H. Qin, Y. He, P. Xu, D. Huang, Z. Wang, H. Wang, Z. Wang, Y. Zhao, Q. Tian, C. Wang, Spinel ferrites (MFe2O4): synthesis, improvement and catalytic application in environment and energy field, Adv. Colloid Interface Sci. 294 (2021) 102486.
[72] S.A. Ansari, A. Nisar, B. Fatma, W. Khan, A.H. Naqvi, 2012. Investigation on structural, optical and dielectric properties of Co doped ZnO nanoparticles synthesized by gel-combustion route, Mater. Sci. Eng.: B 177 (5) (2012) 428–435.